

Control of interfacial pH in mesoporous silica nanoparticles via surface functionalization

Dilini Singappuli-Arachchige,^{1,2} and Igor I. Slowing^{1,2,a)}

¹US DOE Ames Laboratory, Ames, Iowa 50011, United States

²Department of Chemistry, Iowa State University, Ames, Iowa 50011, United States

a) Electronic mail: islowing@iastate.edu

ABSTRACT

The pH at silica-water interfaces (pH_{int}) was measured by grafting a dual emission fluorescent probe (SNARF) onto the surface of mesoporous silica nanoparticles (MSN). The values of pH_{int} of SNARF-MSN suspended in water were different from the pH of the bulk solution (pH_{bulk}). Addition of acid or base to aqueous suspensions of SNARF-MSN induced much larger changes in pH_{bulk} than pH_{int} , indicating that the interface has buffering capacity. Grafting additional organic functional groups onto the surface of SNARF-MSN controls the pH_{int} of its buffering region. The responses of pH_{int} to variations in pH_{bulk} are consistent with the acid/base properties of the surface groups as determined by their pK_a and are affected by electrostatic interactions between charged interfacial species as evidenced by the dependence of ζ -potential on pH_{bulk} . Finally, as a proof of principle, we demonstrate that the hydrolysis rate of an acid-sensitive acetal can be controlled by adjusting pH_{int} via suitable functionalization of the MSN surface. Our findings can lead to the development of nanoreactors that protect sensitive species from adverse conditions and tune their chemical reactivity.

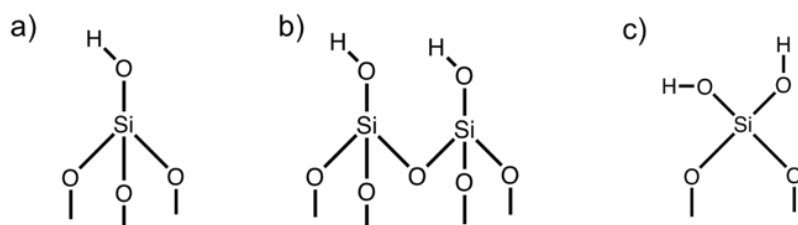
I. INTRODUCTION

The properties of the silica-water interface are determined by the surface chemistry of silica and can differ significantly from those of the bulk solvent.¹⁻⁷ Of particular relevance is how surface moieties can affect the acidity or basicity of the interface, because proton transfer processes are involved in a large number of reactions and can affect the stability and behavior of adsorbed chemical species.⁸⁻¹² Several groups have explored the acid-base properties of mesoporous silica-water interfaces using different approaches including electrochemical and conductivity measurements,^{13, 14} permeability and adsorption of acids or bases,^{15, 16} and spectroscopic methods.¹⁷⁻²² These studies have demonstrated that the pH at the silica-water interface is different from that of the bulk.^{15, 17-19, 21} This difference suggests the possibility of adjusting the interfacial pH to target values. Attaining such control would enable regulating pH sensitive transformations at interfaces and protecting surface species from unfavorable conditions.

The acid-base properties of silica derive from their weakly acidic silanol groups (Si-OH), which can be either isolated or H-bonded with neighboring silanols. The H-bonded silanols can belong to the same (geminal) or different (vicinal) Si atoms (Scheme 1). Ong et al. used second harmonic generation measurements to probe these groups at the silica-water interface.²³ They observed that at pH > 4 the negatively charged surface produces an electric field that polarizes the interfacial water molecules to give a frequency doubling, and used this property to track deprotonated sites. They reported that a fused silica surface contains two types of silanols with different acidities: ca. 19% with a pK_a 4.5, and 81% with a pK_a 8.5. However, the origin of this bimodal distribution was unclear.

Later studies proposed that the lower pK_a corresponded to isolated silanols, and the higher to H-bonded silanols (geminal and vicinal).²⁴⁻²⁶

Scheme 1. Types of silanol groups on silica surfaces: a) isolated b) vicinal and c) geminal.



Rosenholm et al. studied the adsorption of benzylamine from solution onto non-functionalized and carboxylic acid-modified SBA-15 as a function of pH. The adsorption isotherms were used to calculate apparent pK_a values for surface silanols and carboxylic groups.¹⁵ They identified two types of silanols for non-modified silica ($pK_{a1} < 2$, $pK_{a2} = 8.2$) and an additional pK_a value (4.8) in the modified material, which was assigned to the surface carboxylic groups. They related the effective proton concentration at the pore surface to the bulk proton concentration through the expression:

$$pH_s = pH_b + \frac{2.3\Psi e}{kT} \quad (1)$$

where Ψ is the surface potential, e is the unit charge, k is the Boltzmann constant and T is the temperature. They suggested that confinement inside the pore leads to an overlap between the electrostatic potential fields of the negative surface charges and inhibits silanol deprotonation. This results in a decreased effective acidity, i.e. a higher apparent pK_a . O'Reilly and co-workers further suggested that protons from the bulk are attracted to the densely charged silica surface thus inducing a difference between interfacial and bulk pH.²⁷ Teramae and co-workers studied the acid-base equilibria in a mesoporous silica densely functionalized with amine groups using adsorbed fluorescence pH indicators. The

fluorescence spectra provided direct information about the molar ratios of neutral, dissociated and protonated forms of the dyes, which in turn gave information about the effective proton concentrations of their environments.¹⁸ Their results showed a non-linear relationship between the interfacial and bulk pH values, in which large variations of the solution pH induced only small changes in the interfacial pH. Similarly, Desai et al. observed that while the fluorescence intensity of fluorescein-labeled mesoporous silica nanoparticles (MSN) increased with the pH of the solution, adsorbing polyethyleneimine onto the material resulted in a fluorescence intensity that did not change with solution pH.²⁸ Olsson and co-workers designed another method to measure pH inside the pores of SBA-15 type mesoporous silica by immobilizing a fluorescently labeled acid-sensitive protein on the material. They showed that the pH inside the pores remained close to 7 while they varied the solution pH in the range 6-8, concluding that the pores had a buffering capacity.¹⁹

All these studies indicate that the pH in the vicinity of the silica surface is different from the bulk and suggest that controlling the surface chemistry of this material could be a powerful tool for adjusting the interfacial pH to desired values. Herein we demonstrate that the interfacial pH of mesoporous silica nanoparticles (MSN) can be fine-tuned by immobilizing acidic or basic groups on their surface. We synthesized a series of organo-functionalized MSN containing the pH sensitive ratiometric probe Carboxy-SNARF (2-(10-(dimethylamino)-3-oxo-3H-benzo[c]xanthen-7-yl)-1,5-benzenedicarboxylic acid). The materials were suspended in water, titrated with HCl and NaOH, and their interfacial pH (deduced from the Carboxy-SNARF fluorescence) were compared to the pH of the bulk solution. We found that the interfacial pH depends on the pK_a of the grafted species and

the ionic strength of the solution. We then showed that controlling the interfacial pH by grafting organic groups on MSN can be used to regulate chemical processes, such as the rate of hydrolysis of an acetal grafted on the silica surface.

II. EXPERIMENTAL

A. Materials

A.1. Chemical precursors: Hexadecyltrimethylammonium bromide (CTAB), methanol, N-(3-dimethylaminopropyl)-N'-ethylcarbodiimidehydrochloride, N-hydroxysuccinimide sodium salt and hexane were purchased from Sigma-Aldrich. Tetraethylorthosilane (TEOS), 3-aminopropyl trimethoxysilane, N'-[3-(trimethoxysilyl)propyl]ethylenediamine, N'-[3-(trimethoxysilyl)propyl]diethylenetriamine, and 3-(trimethoxysilyl)propylsuccinic anhydride were purchased from Gelest, Inc. NaOH, NaCl, concentrated HCl, methylene chloride, ethyl acetate and acetone were purchased from Fisher Scientific. 5-(and-6)-Carboxy SNARF-1 was purchased from Invitrogen by Thermo Fisher Scientific. All reagents were used as received without further purification.

A.2. Synthesis of MCM-41 type Mesoporous Silica Nanoparticles (MSN): CTAB (1.0 g, 2.74 mmol) was dissolved in deionized water (480 mL) in a round bottom flask followed by addition of 2M NaOH (3.5 mL, 7.0 mmol). The solution was continuously stirred for one hour at 80 °C. Tetraethylorthosilicate (TEOS, 5.0 mL, 22.6 mmol) was then added dropwise over 5 min to the CTAB solution. Magnetic stirring was continued for additional 2 h at 80 °C. The solution was filtered, washed with abundant water and methanol. CTAB template was removed by calcination of dry solid at 550 °C for 6 h with a rate of 2 °C/min.

The material was characterized by nitrogen physisorption isotherms and XRD patterns (Figure S1).

A.3. Synthesis of functionalized SNARF-MSN: 5-(and-6)-Carboxy SNARF-1 (1 mg, 2.2 μmol) was added to excess N,N'-dicyclohexylcarbodiimide (3 mg, 15 μmol) in methylene chloride (0.5 mL) followed by N-hydroxysuccinimide (3 mg, 26 μmol). The reagents were stirred at 25 °C for 24 h. Aminopropyltrimethoxysilane in acetone (30 mM, 0.100 mL) was added to the mixture and continued stirring at 25 °C for another 24 h. The solvent was removed under reduced pressure, resultant SNARF-AP-TMS was redissolved in acetone, an aliquot of the solution (1.1 mM, 1.0 mL) was added to pre-calcined MSN (1.0 g) and ground until seemingly dry. The material was then heated in a microwave reactor at 100 °C for 30 min, washed with water until supernatant showed no fluorescence and vacuum dried overnight. The resultant material termed SNARF-MSN was then impregnated with different organosilanes via incipient wetness. Organosilanes dissolved in acetone (1M, 0.100 mL) were added to SNARF-MSN (0.100 g) separately and ground until seemingly dry. The material was then heated in a microwave reactor at 100 °C for 30 min, washed with water and vacuum dried overnight. The target loadings were 1 mmol/g for all materials, except for SA/DAP-SNARF-MSN that had 0.5 mmol/g target loading for each group. The materials were washed with water and vacuum dried overnight. The materials were characterized by DRIFT spectroscopy and elemental analysis.

A.4. Synthesis of SNARF-AP: 5-(and-6)-Carboxy SNARF-1 (0.25 mg, 0.55 μmol) was added to excess N,N'-dicyclohexylcarbodiimide (0.75 mg, 3.75 μmol) in methylene chloride (0.125 mL) followed by N-hydroxysuccinimide (0.75 mg, 6.5 μmol). The reagents were stirred at 25 °C for 24 h. Propylamine in acetone (75 mM, 0.010 mL) was added to

the mixture and continued stirring at 25 °C for another 24 h. The resultant SNARF-AP was separated via thin layer chromatography using ethylacetate:hexane (3:1) as the mobile phase. The silica layer was scratched, and SNARF-AP was extracted to ethanol. The solvent was removed under reduced pressure. The product was characterized by DRIFT spectroscopy and mass spectrometry.

A.5. Synthesis of functionalized MSN-PNB: A solution of 5,6-epoxyhexyltriethoxysilane in ethanol (0.5 mL, 0.4 M) was added to pre-calcined MSN (500 mg) and ground until seemingly dry. The material was then heated in a microwave reactor at 100 °C for 2 h, washed with water and vacuum dried. The resultant material was suspended in water (10 mL) followed by addition of H₂SO₄ (0.5 mL, 0.1 M). The mixture was heated at 85 °C for 3 h, washed with water and vacuum dried. The resultant product was re-suspended in ethanol (30 mL), followed by addition of *p*-nitrobenzaldehyde (0.40 mmol, 60 mg) and H₂SO₄ (0.5 mL, 0.1 M). The mixture was then heated at 85 °C for 5 h, washed with ethanol and vacuum dried. The resultant MSN-PNB was characterized by DRIFT-IR and elemental analysis. The PNB acetal loading in the material was 0.02 mmol/g. MSN-PNB was then impregnated with 3-(trimethoxysilyl)propylsuccinic anhydride and N'-[3-(trimethoxysilyl)propyl]diethylenetriamine via incipient wetness: the organosilanes dissolved in anhydrous ethanol (1M, 0.070 mL) were added to MSN-PNB (0.070 g) separately and ground until seemingly dry. The material was then heated in a microwave reactor at 100 °C for 30 min, washed with ethanol and vacuum dried overnight. All the materials were characterized by elemental analysis and DRIFT spectroscopy. Both propyl-succinic anhydride and diethylenetriamine loadings were 0.7 mmol/g each as determined by elemental (C,H,N) analysis.

B. Methods

B.1. Characterization: A Rigaku-Ultima 4 X-ray diffractometer equipped with Cu K α radiation (40 kV, 44 mA) was used to record XRD patterns over the range of 1–5 2 θ degrees. A Micromeritics Tristar surface area and porosity analyzer was used to measure nitrogen sorption isotherms. The surface areas and pore size distributions were calculated using the Brunauer-Emmett-Teller (BET) and Barrett-Joyner-Halenda (BJH) methods respectively. Elemental analyses of different MSN samples were done by triplicate on a Perkin Elmer 2100 series II CHNS analyzer, using acetanilide as calibration standard and combustion and reduction temperatures of 925 °C and 640 °C respectively. Diffuse Reflectance Infrared Fourier Transform (DRIFT) measurements were done using a Bruker Vertex 80 FT-IR spectrometer equipped with a HeNe laser, photovoltaic MCT detector and OPUS software. Fluorescence spectra were acquired on a Cary Eclipse fluorescence spectrophotometer. Excitation wavelength was set at 488 nm, both excitation and emission slit widths were set at 5 nm. Positive ion mode mass spectra (MS) were obtained using an Agilent QTOF 6540 mass spectrometer. The instrument was operated in the 4 GHz HRes mode. Accurate mass measurements were achieved by constantly infusing a calibrant (masses 121.0508 and 922.0098).

B.2. Titrations of functionalized SNARF-MSN and SNARF-AP: Functionalized SNARF-MSN materials were suspended in water (5 mg/mL, 5.0 mL) and titrated with aqueous HCl (5 mM) and aqueous NaOH (5 mM) separately. At each addition of acid/base, the pH of solution was measured using a pH meter and fluorescence spectra of the suspension was recorded using Cary Eclipse fluorescence spectrophotometer. SNARF-AP (0.3 mg) was added to aqueous NaOH (5 mM) and titrated against aqueous HCl (5 mM). At each addition of acid/base, the pH of solution was measured using a bench-top pH meter and fluorescence spectra of the suspension was recorded using Cary Eclipse fluorescence spectrophotometer. The fluorescence intensity ratio (588 nm/635 nm) was plotted against the measured solution pH.

B.3. Hydrolysis of PNB acetal: Functionalized MSN-PNB samples (25.0 mg each) were introduced into a dialysis membrane (Spectrum Labs, MW cutoff = 12-14 kDa) and immersed into an aqueous HCl solution of pH 5 (10.0 mL). The intact aqueous solution was continuously circulated through a quartz flow cuvette as described in a previous work,²⁹ and the absorption band at 274 nm was monitored for 7 h via UV-vis spectroscopy, taking scans every 5 min. Three separate hydrolysis experiments were performed for each material, and the results were averaged.

III. RESULTS AND DISCUSSION

A. Synthesis of functionalized SNARF-MSN and SNARF-AP

We first reacted the dual emission pH responsive probe Carboxy-SNARF-1^{19, 30} (C-SNARF, 2.2 μ mol) with 3-aminopropyltrimethoxysilane (AP-TMS, 3 μ mol) via dicyclohexylcarbodiimide /N-hydroxysuccinimide (DCC/NHS) coupling (25 °C, 24 h). The

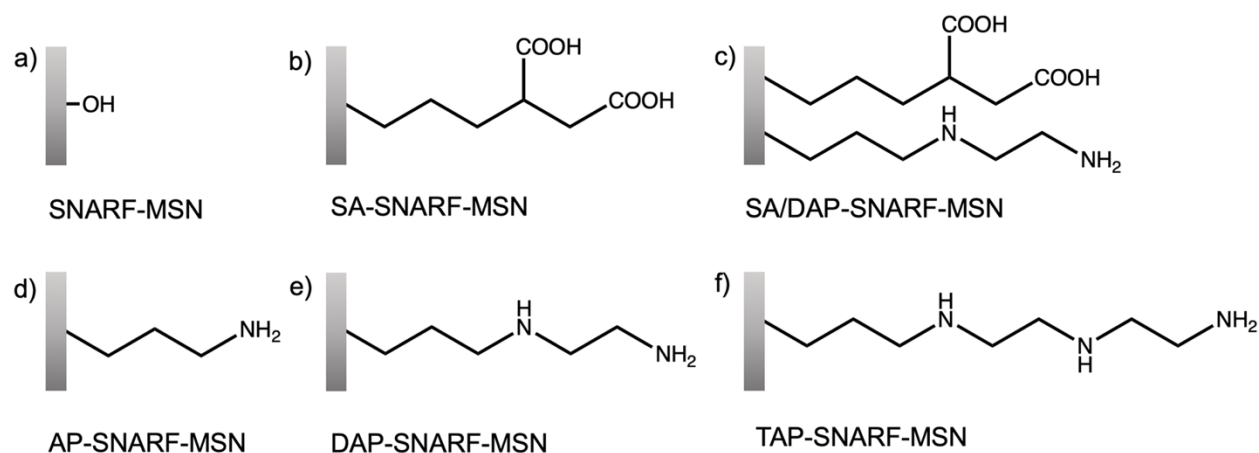
resultant SNARF-AP-TMS was grafted onto pre-calcined mesoporous silica nanoparticles (MSN, characterization in Figure S1). The material was termed SNARF-MSN. Then, we produced a set of surface-functionalized materials by grafting organosilanes with groups of different pK_a values onto SNARF-MSN (Scheme 2, Table S1).

Successful grafting of the groups was verified by DRIFT spectroscopy and elemental analysis (Table S1, Figures S2). Characteristic features in the IR spectra include C-H stretching bands in the range $2850\text{-}2950\text{ cm}^{-1}$ and C-H bending modes in the range $1440\text{-}1560\text{ cm}^{-1}$ for all samples, vibration bands attributed to C-N stretching at 1365 cm^{-1} for AP-, DAP-, TAP- and SA/DAP-SNARF-MSN, C=O stretching at 1725 cm^{-1} and C-O stretching at 1380 cm^{-1} for both SA- and SA/DAP-SNARF-MSN. Elemental analysis indicated the group loadings were in the range $0.7\text{-}0.8\text{ mmol/g}$ for all monofunctional samples and the bifunctional SA/DAP-SNARF-MSN had 0.4 mmol/g and 0.3 mmol/g loading of each group respectively.

We also coupled C-SNARF with propyl amine via DCC/NHS reaction ($25\text{ }^\circ\text{C}$, 24 h) to produce a homogeneous analog of SNARF-AP-TMS. The compound was designated as SNARF-AP, and was used to build a calibration plot of fluorescence intensity ratios (I_{588}/I_{635}) versus solution pH. This compound was characterized by FTIR and mass spectroscopy (Figures S3, S4). C-SNARF and SNARF-AP both showed characteristic bands for O-H ($3100\text{-}3700\text{ cm}^{-1}$), C-H ($2850\text{-}3000\text{ cm}^{-1}$), aromatic C=C ($1300\text{-}1500\text{ cm}^{-1}$), and C-O (1074 cm^{-1}) stretches and =C-H bend ($735\text{-}870\text{ cm}^{-1}$). C-SNARF showed a broad band centered around 1640 cm^{-1} , which likely corresponds to the overlapping bands of the C=O stretches of the two carboxylic groups. SNARF-AP showed characteristic amide bands (absent in C-SNARF) that include amide I band corresponding

to amide C=O stretch (1697 cm^{-1}), amide II band (N-H bend, 1617 cm^{-1}), amide III (C-N stretch and N-H in plane deformation 1207 cm^{-1}) and amide IV (in plane amide C=O bend and C-C stretch, 764 cm^{-1}).³¹ In addition, mass spectra showed the parent peaks of SNARF at $m/z=454\text{ [M-H]}^+$ and AP-SNARF at $m/z=495\text{ [M-H]}^+$. These results confirmed that the AP modification of C-SNARF was successful.

Scheme 2. Structures of the functional groups added to the surface of SNARF-MSN.



B. Acid-Base Titrations of SNARF-MSN

B.1 Calibration curve for pH_{int}

The protonated and deprotonated forms of the SNARF-AP showed two fluorescence emission maxima (588 nm and 635 nm, respectively) when excited at 488 nm (Figure 1a). The ratio of the fluorescence intensities at these wavelengths (I_{588}/I_{635}) provides a measure of the pH of the probe's environment.¹⁹ To construct a calibration plot, we titrated an aqueous solution of SNARF-AP in NaOH (5 mM, 5 mL) with aqueous HCl (5 mM). The fluorescence spectra and the pH of the solution (measured with a pH meter) were collected following each addition of the titrant. The sigmoidal plot showed a

decrease in intensity ratio (I_{588}/I_{635}) with increasing pH (Figure 1b), which is consistent with previous reports of free and bound SNARF.³⁰ The linear range of the plot is limited to fluorescence intensity ratios between 0.2 and 2.0, corresponding to solution pH values of 9.3 to 6.5 respectively (Figures 1b, S5). The regression equation of the linear plot was used to calculate the pH at the interface of aqueous suspensions of SNARF-modified MSN. Hereafter, the pH of the bulk solution is termed pH_{bulk} and the pH at the silica-water interface is termed pH_{int} .

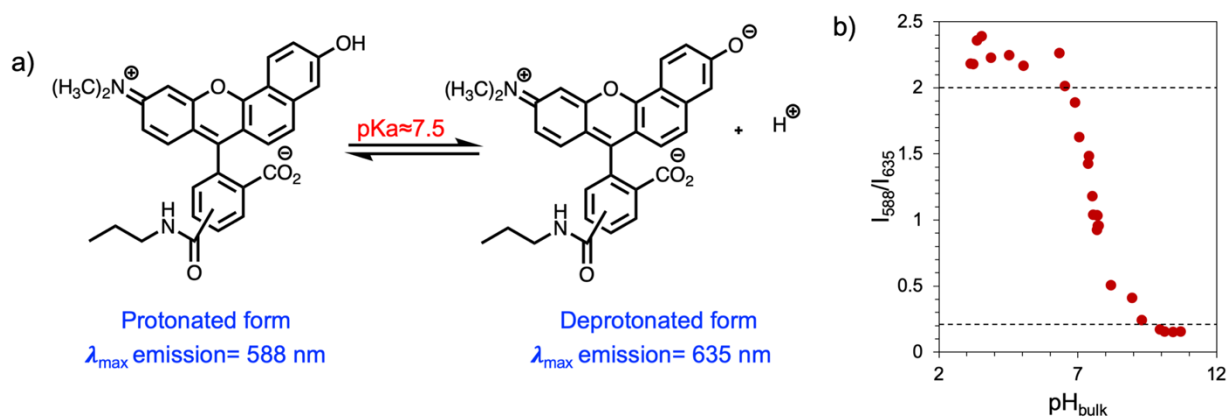


Figure 1. a) Protonated and deprotonated states of SNARF-AP.¹² b) Titration curve of SNARF-AP displaying the change of I_{588}/I_{635} as a function of pH_{bulk} .

B.2. Titrations of non-functionalized and functionalized SNARF-MSN

The aqueous suspensions of functionalized-SNARF-MSN materials (5.0 mg/mL) were titrated with HCl (5.0 mM) or NaOH (5.0 mM) solutions. Each titrant addition was followed by pH_{bulk} measurement (using a pH meter) and recording of the fluorescence spectrum (Figure S6). The I_{588}/I_{635} decreased with increasing pH_{bulk} for all of the samples (Figure S7). Data analysis was restricted to fluorescence intensity ratios in the linear region of the SNARF-AP calibration ($I_{588}/I_{635} = 2.0 - 0.2$), corresponding to interfacial pH

(pH_{int}) values in the range 6.5 to 9.3 (Figure S5). Consistent with previous reports, all pH_{int} were different from pH_{bulk} .¹⁸ Interestingly, the relationship between both pH values was not linear and varied with the nature of the functional groups in the materials (Figure 2a). Two regions can be identified in Figure 2a for all of the samples: one at low pH_{bulk} where the interface is less acidic than the bulk ($\text{pH}_{\text{int}} > \text{pH}_{\text{bulk}}$), and one at high pH_{bulk} where the interface is less basic than the bulk ($\text{pH}_{\text{int}} < \text{pH}_{\text{bulk}}$). Importantly, variations in pH_{int} were significantly smaller than those in pH_{bulk} : for a bulk pH change of 6 units the pH_{int} change was only ca. 1.5 units for all the functionalized SNARF-MSN materials. This suggests that all the interfaces were buffered. Furthermore, the buffering effect varied with the type of functionality in the materials.

In general, for any given pH_{bulk} value pH_{int} increased in the order SA-SNARF-MSN \lesssim SNARF-MSN < SA/DAP-SNARF-MSN < AP-SNARF-MSN < DAP-SNARF-MSN < TAP-SNARF-MSN (Table S1). This trend corresponds with the type of functional acid/base groups in the material: while SA groups increased the acidity of the interface, amine groups made it more basic. pH_{int} also increased with the number of amine groups in the organic chain (AP < DAP < TAP). A combination of SA and DAP groups gave pH_{int} values in between those of the acid and base functionalized materials. Notably, the shapes of the pH_{bulk} versus pH_{int} curves are different for acidic than for basic groups. The shapes of these curves indicate that: 1) pH_{int} of the materials with acidic surfaces (SA-SNARF-MSN and SNARF-MSN) has little variation in the acid pH_{bulk} region (pH_{bulk} 3 – 7, i.e. a buffer behavior), but a sharper response to pH_{bulk} in the basic region ($\text{pH}_{\text{bulk}} > 7$); and 2) pH_{int} of the materials with basic groups (AP-, DAP- and TAP-SNARF-MSN) display larger variation in the acidic pH_{bulk} regime, that tends to plateau in the basic pH_{bulk} region.

Interestingly, SA/DAP-SNARF-MSN having both acidic and basic groups showed a more complex behavior, with steeper pH_{int} changes in the acid and basic regions ($pH_{bulk} < 4.5$ and >7.5 respectively), and a buffering zone of nearly constant pH_{int} in between. These results may be understood by considering the acid-base equilibria of the surface groups (Figure S8) and the effect of surface charge on the activity of ions at the interface according to the Debye-Hückel theory.

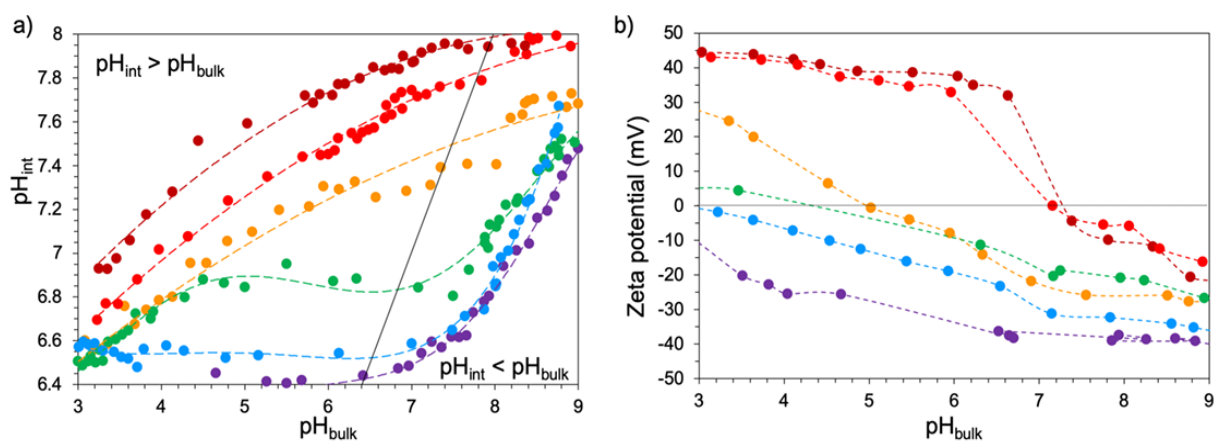


Figure 2. a) Variation of a) pH_{int} and b) ζ -potential with pH_{bulk} for functionalized SNARF-MSN. The diagonal in a) corresponds to $pH_{int} = pH_{bulk}$. Discontinuous lines in a) are only visual aids. TAP-SNARF-MSN (burgundy), DAP-SNARF-MSN (red), AP-SNARF-MSN (orange), SA/DAP-SNARF-MSN (green), SNARF-MSN (blue), SA-SNARF-MSN (purple).

B.3. Interfacial acid-base equilibria of functionalized SNARF-MSN

Because SNARF loading is too small (1 $\mu\text{mol/g}$) compared to the number of silanols and functional groups in the materials (ca. 3.0 and 0.8 mmol/g respectively) the contribution of SNARF protonation/deprotonation equilibrium to pH_{int} can be neglected. Therefore, the only relevant acid-base equilibria in the materials are the protonation/deprotonation of silanols and surface organic groups.

When titrating the silanols in SNARF-MSN from low to high pH, the surface charge of the material becomes increasingly negative due to silanoxy ion formation. The development of anionic groups on the surface is evidenced by the continuous drop in the ζ -potential of the material (from 0 to -35 mV) when pH_{bulk} is varied from 2 to 9 (Figure 2b). The surface silanol density in MSN is ca. 4 groups/ nm^2 ,³² and corresponds to average inter-silanol distances ca. 0.5 nm, which are much smaller than the Debye radius for aqueous solutions of electrolytes at the titrant concentration (4.3 nm at 5 mM).³³ Thus, the proximity between silanol groups inhibits their dissociation due to the strong coulombic repulsion between the resulting silanoxy anions (Figure 3a). This shift in equilibrium implies a lower H^+ activity at the interface compared to the bulk and explains the $\text{pH}_{\text{int}} > \text{pH}_{\text{bulk}}$ observed in the acidic region of the titration curve (pH_{bulk} 3 – 7). In contrast, in the basic region $\text{pH}_{\text{int}} < \text{pH}_{\text{bulk}}$, with both pH increasing at comparable rates (although pH_{int} is lagged). The different behavior of pH_{int} in the basic region is attributed to dissociation of the more weakly acidic H-bonded silanols (pK_a 8.5) along with silanoxy anion stabilization via charge screening by Na^+ counterions from the titrant (Figure 3b). According to the Gouy-Chapman-Stern theory, the difference in potential between the charged surface and the bulk liquid induces migration of ions towards the SNARF-MSN particles to form an electric double layer, thereby establishing a higher cation concentration at the interface than the bulk.^{27, 34-36} A similar behavior is observed for SA-SNARF-MSN. However, because of its lower pK_a (4.2 versus 4.5 for isolated silanols) the buffered region appears at a slightly lower pH.

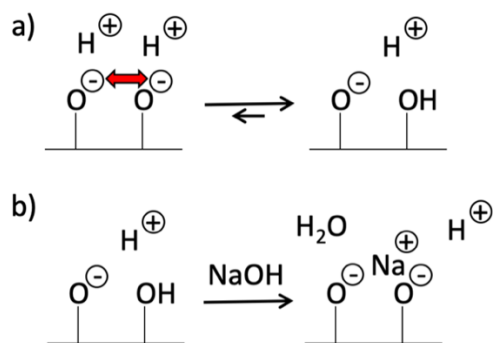


Figure 3. a) Inhibition of silanol dissociation at low pH due to charge repulsion, and b) enhancement of silanol dissociation at high pH (reaction with NaOH) due to charge screening by Na⁺ counterions.

The effect of basic groups on the pH_{int} of functionalized SNARF-MSN is much more dramatic than that of the succinic acid groups. In the acidic region ($\text{pH}_{\text{bulk}} < 7$) amine groups in AP-, DAP- and TAP-SNARF-MSN act as proton scavengers and become alkylammonium cations as evidenced by the positive ζ -potentials of the materials (Figure 2b). The densely charged surface is stabilized by ion pair formation with silanoxo groups and screening by chloride counterions from the titrant (Figure 4a). Thus, the free $[\text{H}^+]$ is lower at this interface than at the solvent-silica interface of SNARF-MSN or SA-SNARF-MSN, and the bulk solution ($\text{pH}_{\text{int AP-SNARF-MSN}} > \text{pH}_{\text{int SNARF-MSN}} > \text{pH}_{\text{bulk}}$). Raising the pH_{bulk} leads to a decrease in ζ -potentials to reach neutrality at pH_{bulk} 5, 7.1 and 7.3 for AP-, DAP- and TAP-SNARF-MSN, respectively. These points of zero charge (PZC) vary as a function of the number of N atoms in the organic groups (AP \ll DAP $<$ TAP) and the pK_a of the corresponding alkylammonium ions. For these materials the drop in ζ -potential is a combination of alkylammonium and silanol deprotonation corresponding to loss of positive and gain of negative surface charges, respectively. It is noteworthy that the first

ammonium group in TAP is as acidic as the isolated silanols (pK_a 4.5).³⁷ At the PZC the number of protonated alkylammonium groups matches the number of deprotonated silanoxy groups on the functionalized SNARF-MSN surfaces. The rate of increase in pH_{int} for these materials is lower than pH_{bulk} , and drops steadily suggesting that a plateau may be reached at $pH_{bulk} > 8$. The decreasing pH_{int} sensitivity to the addition of base titrant suggests that the incoming OH^- are neutralized by H^+ from alkylammonium surface groups, while Na^+ take over as counterions for silanoxy stabilization (Figure 4b). The combination of silanoxy stabilization and alkylammonium deprotonation also results in increasingly negative ζ -potentials.

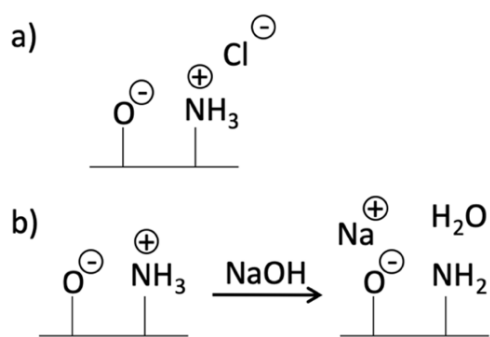


Figure 4. a) Amine protonation decreases the effective $[H^+]$ in the acidic region of the titration curve, the resulting ammonium ions are stabilized by silanoxy or Cl^- counterions. b) Added base has little effect on pH_{int} because it is neutralized via deprotonation of the surface ammonium ions.

The dependence of pH_{int} of SA/DAP-SNARF-MSN on pH_{bulk} appears as a combination of those of the individual SA- and DAP-SNARF-MSN materials. The behavior in the low pH region ($pH_{bulk} < 4.5$) is dominated by the basic component (DAP) with a small excess of protonated alkylammonium groups indicated by the slightly positive ζ -potential. In this first regime pH_{int} is higher than pH_{bulk} likely due to stabilization of

protonated alkylammonium by carboxy, silanoxy and chloride counterions. Furthermore, the rate of pH_{int} increase with pH_{bulk} is the same as that of the amine functionalized SNARF-MSN materials. Upon reaching the PZC ($\text{pH}_{\text{bulk}} \sim 4.5$) the pH_{int} becomes invariant at ca. 6.9 over a range of 3 pH_{bulk} units (4.5 – 7.5). In this regime, the interface behaves like a traditional buffer due to coexistence of acidic (carboxylic, silanol) and basic (amine) groups with pK_a spanning from 4.2 to 7.5. At higher pH, the behavior resembles that of acidic MSN materials, with a sharp increase in pH_{int} trailing pH_{bulk} by about one unit, and the silanoxy and carboxy surface charges stabilized via screening by Na^+ counterions from the titrant.

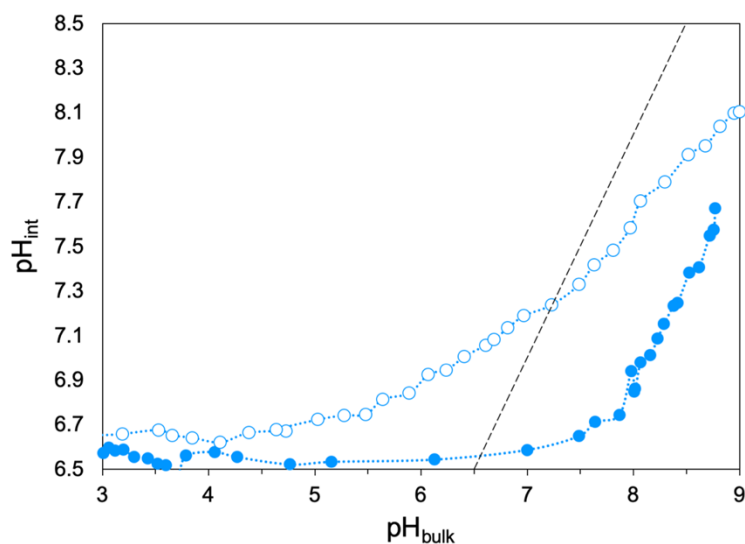


Figure 5. Effect of ionic strength on the dependence of pH_{int} on pH_{bulk} for SNARF-MSN. Titration of the material in water (filled circles) and 1M NaCl solution (empty circles). Discontinuous line represents $\text{pH}_{\text{int}} = \text{pH}_{\text{bulk}}$.

The above discussion suggests that coulombic interactions at the MSN surface play a critical role in regulating pH_{int} . Indeed, increasing the ionic strength of the solution

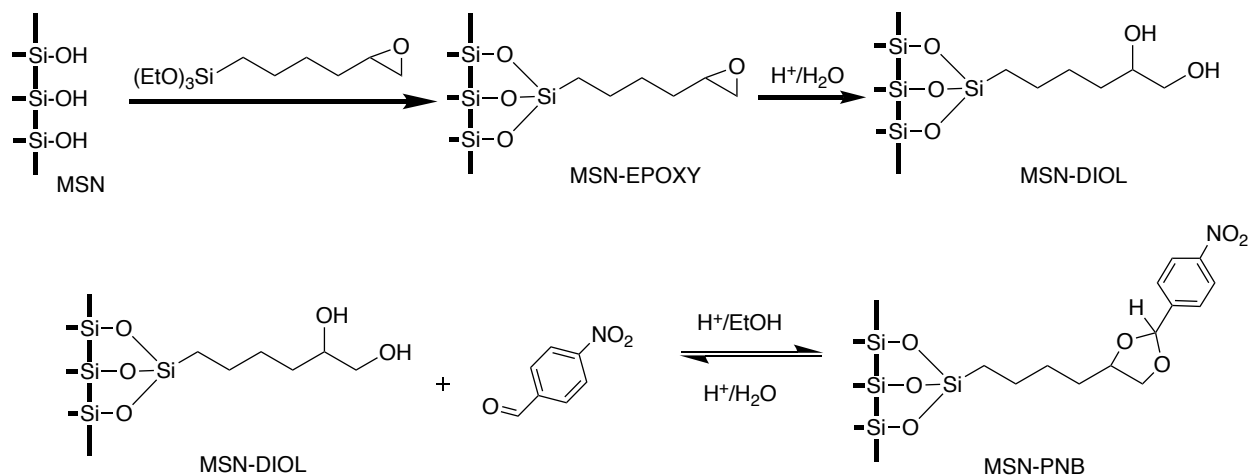
by adding NaCl (1M) to the solvent results in larger differences between pH_{int} and pH_{bulk} for SNARF-MSN in the acidic range but smaller changes in the neutral and moderately basic pH regime (Figures 5, S9). Thus, screening of surface charges by counterions appears to be much more relevant in the neutral to basic region than in the acidic range, where the higher ionic strength leads to low H^+ activities at the interface (i.e. higher pH_{int}). The larger effect of ionic strength on the stability of surface charges in the basic region has been previously reported.³⁸ Importantly, increasing the ionic strength of the solution decreases the material's capacity to resist pH_{int} changes in the 4.5 – 7 pH_{bulk} regime. However, the change in pH_{int} (ca. 0.5 units) is still much smaller than that of the bulk.

C. Controlling the hydrolysis of *p*-nitrobenzaldehyde-acetal

To evaluate the buffering activity of the functionalized MSN-water interfaces we examined their capacity for inhibiting the hydrolysis of an acetal in aqueous HCl. We synthesized a parent material with *p*-nitrobenzaldehyde (PNB) moiety bound to a surface organic group via an acetal linkage (MSN-PNB, Scheme 3). The material was then further grafted with acidic and basic silanes to produce the corresponding SA-MSN-PNB and TAP-MSN-PNB. All materials were characterized by DRIFT spectroscopy and showed the characteristic NO_2 stretching signals (1525 cm^{-1} and 1350 cm^{-1}) confirming the incorporation of the target molecule. Importantly, the carbonyl stretch (1700 cm^{-1}) of PNB was absent in all synthesized materials. In contrast, a control sample prepared by physically adsorbing PNB on MSN showed characteristic IR bands for C=O stretch (1700 cm^{-1}) along with the two NO_2 stretching signals (1525 cm^{-1} and 1350 cm^{-1}) (Figure S10).

These observations suggested the successful formation of the acetal linkage. Elemental analysis indicated PNB loading in the parent MSN-PNB sample was 0.02 mmol/g.

Scheme 3. Synthesis of MSN-PNB.



The MSN-PNB samples (25.0 mg each) were then set in a dialysis bag and immersed in an aqueous solution with pH_{bulk} adjusted to 5 (10.0 mL) at 25 °C to induce the hydrolysis of the acetal. The production of PNB was tracked by UV-visible spectroscopy measuring the absorbance at 274 nm (Figure 6). In spite of having the same pH_{bulk} the rates of *p*-nitrobenzaldehyde production varied between the different MSN-PNB materials. Because the rate of acetal hydrolysis decreases with increasing pH ,³⁹ this result suggests that the pH in the immediate environment of the immobilized acetal (i.e. pH_{int}) is different for each material. Indeed, the rates of hydrolysis decreased in the order SA-MSN-PNB > MSN-PNB > TAP-MSN-PNB, which corresponds to increasing pH_{int} of the materials (for $\text{pH}_{\text{bulk}} = 5$, the corresponding pH_{int} are <6.5, 6.5 and 7.5 respectively, Figure 2a), confirming that the pH of the local environment was effectively regulated by the surface chemistry of the materials.

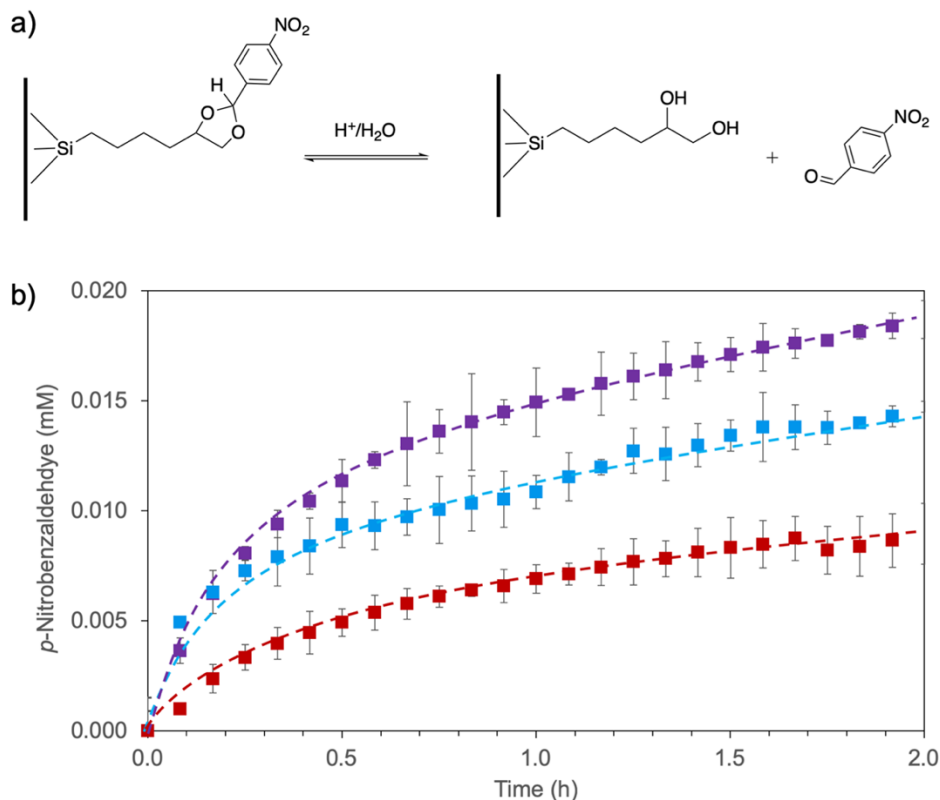


Figure 6. a) Hydrolysis of *p*-nitrobenzaldehyde acetal from the materials under acidic conditions. b) *p*-Nitrobenzaldehyde produced from SA-MSN-PNB (purple), MSN-PNB (blue), and TAP-SNARF-MSN (burgundy) vs time. Dotted lines are only visual aids.

IV. CONCLUSIONS

In summary, the pH_{int} at the mesoporous silica-water interface can be adjusted by grafting acid/base functional groups on the MSN pores. The functionalized materials exhibit buffering capacity at pH values that depend on the pK_{a} of the surface groups, and are different from the pH of the bulk solution. The pH_{int} is also controlled by coulombic interactions between charged surface species, these interactions affect dissociation equilibria, namely decreasing H^+ activities for silanol groups that are separated by distances smaller than the Debye length (<4 nm at 5 mM ionic strength). Surface charges

can be screened by counterions at the interface, thus the ionic strength of the solution impacts pH_{int} and the buffering capacity of the materials. The buffering property of the functionalized pores allows controlling the stability of acid-sensitive surface species. For instance, the rates of hydrolysis of MSN-bound acetals can be regulated by functionalizing the surface with species of varying pK_a . Thus, the rates of PNB acetal hydrolysis depend directly on pH_{int} , rather than pH_{bulk} . Ultimately, surface functionalization of MSN pores with weakly acidic or basic groups can be a powerful tool for designing nanoreactors that provide optimal conditions for performing pH-dependent reactions or to protect labile chemical species and enzymes from drastic changes in the pH of bulk solutions.

SUPPLEMENTARY MATERIAL

See supplementary material for additional tables and schemes, physisorption, XRD, DRIFT spectra, fluorescence spectra and mass spectra.

ACKNOWLEDGEMENTS

This research is supported by the U.S. Department of Energy, Office of Basic Energy Sciences, Division of Chemical Sciences, Geosciences, and Biosciences, through the Ames Laboratory Catalysis Science program. The Ames Laboratory is operated for the U.S. Department of Energy by Iowa State University under Contract No. DE-AC02-07CH11358.

APPENDIX

List of abbreviations

SNARF – Seminaphtharhodafluor

C-SNARF – Carboxy seminaphtharhodafluor

SNARF-AP-TMS – Seminaphtharhodafluor modified aminopropyl-trimethoxysilane

SNARF-AP – Seminaphtharhodafluor modified propylamine

MSN – Mesoporous silica nanoparticles

SBA-15 – Santa Barbara Amorphous-15 mesoporous silica material

SNARF-MSN – SNARF grafted on MSN

AP-SNARF-MSN – Aminopropyl-modified SNARF-MSN

DAP-SNARF-MSN – 3-(ethylenediamine)propyl-modified SNARF-MSN

TAP-SNARF-MSN – 3-(diethylenetriamine)propyl-modified SNARF-MSN

SA-SNARF-MSN – Succinic acid-modified SNARF-MSN

SA/DAP-SNARF-MSN – Succinic acid and 3-(ethylenediamine)propyl-modified SNARF-MSN

MSN-PNB – Mesoporous silica nanoparticles containing p-nitrobenzaldehyde acetal

SA-MSN-PNB – Succinic acid-modified MSN-PNB

TAP-MSN-PNB- 3-(diethylenetriamine)propyl-modified MSN-PNB

PZC – Point of zero charge

CTAB – Hexadecyltriethylammonium bromide

TEOS – Tetraethylorthosilane

AP-TMS – 3-Aminopropyltrimethoxysilane

DCC/NHS – Dicyclohexylcarbodiimide /N-hydroxysuccinimide

REFERENCES

¹ N. Giovambattista, P. G. Debenedetti, and P. J. Rossky, *J. Phys. Chem. B* **111**, 9581 (2007).

² D. Singappuli-Arachchige, J. S. Manzano, L. M. Sherman, and I. I. Slowing, *ChemPhysChem* **17**, 2982 (2016).

³ A. De Vylder, J. Lauwaert, D. Esquivel, D. Poelman, J. De Clercq, P. Van Der Voort, and J. W. Thybaut, *J. Catal.* **361**, 51 (2018).

⁴ W. Guo, and J. R. Errington, *J. Phys. Chem. C* **123**, 19649 (2019).

⁵ G. E. Purnell, and R. A. Walker, *J. Chem. Phys.* **150**, 194701 (2019).

⁶ V. Ostroverkhov, G. A. Waychunas, and Y. R. Shen, *Chem. Phys. Lett.* **386**, 144 (2004).

⁷ D. Singappuli-Arachchige, T. Kobayashi, Z. Wang, S. J. Burkhov, E. A. Smith, M. Pruski, and I. I. Slowing, *ACS Catal.* **9**, 5574 (2019).

- ⁸ W. Wang, R. Y. Park, D. H. Meyer, A. Travasset, and D. Vaknin, *Langmuir* **27**, 11917 (2011).
- ⁹ A. A. Venn, E. Tambutté, M. Holcomb, J. Laurent, D. Allemand, and S. Tambutté, *Proc. Natl. Acad. Sci. U. S. A.* **110**, 1634 (2013).
- ¹⁰ J. Lauwaert, E. G. Moschetta, P. Van Der Voort, J. W. Thybaut, C. W. Jones, and G. B. Marin, *J. Catal.* **325**, 19 (2015).
- ¹¹ N. A. Brunelli, and C. W. Jones, *J. Catal.* **308**, 60 (2013).
- ¹² H. Zheng, C.-W. Tai, J. Su, X. Zou, and F. Gao, *Dalton Trans.* **44**, 20186 (2015).
- ¹³ D. Fattakhova-Rohlfing, M. Wark, and J. Rathouský, *Chem. Mater.* **19**, 1640 (2007).
- ¹⁴ S. Fujita, A. Koiwai, M. Kawasumi, and S. Inagaki, *Chem. Mater.* **25**, 1584 (2013).
- ¹⁵ J. M. Rosenholm, T. Czuryzkiewicz, F. Kleitz, J. B. Rosenholm, and M. Lindén, *Langmuir* **23**, 4315 (2007).
- ¹⁶ Q. Gao, W. Xu, Y. Xu, D. Wu, Y. Sun, F. Deng, and W. Shen, *J. Phys. Chem. B* **112**, 2261 (2008).
- ¹⁷ E. G. Kovaleva, L. S. Molochnikov, D. O. Antonov, D. P. Tambasova Stepanova, M. Hartmann, A. N. Tsmokalyuk, A. Marek, and A. I. Smirnov, *J. Phys. Chem. C* **122**, 20527 (2018).
- ¹⁸ A. Yamaguchi, M. Namekawa, T. Kamijo, T. Itoh, and N. Teramae, *Anal. Chem.* **83**, 2939 (2011).
- ¹⁹ C. Thörn, N. Carlsson, H. Gustafsson, K. Holmberg, B. Åkerman, and L. Olsson, *Microporous Mesoporous Mater.* **165**, 240 (2013).
- ²⁰ I. G. Shenderovich, G. Buntkowsky, A. Schreiber, E. Gedat, S. Sharif, J. Albrecht, N. S. Golubev, G. H. Findenegg, and H.-H. Limbach, *J. Phys. Chem. B* **107**, 11924 (2003).
- ²¹ E. G. Kovaleva, L. S. Molochnikov, E. L. Golovkina, M. Hartmann, I. A. Kirilyuk, and I. A. Grigor'ev, *Microporous Mesoporous Mater.* **203**, 1 (2015).
- ²² E. G. Kovaleva, L. S. Molochnikov, E. L. Golovkina, M. Hartmann, I. A. Kirilyuk, and I. A. Grigor'ev, *Microporous Mesoporous Mater.* **179**, 258 (2013).
- ²³ S. Ong, X. Zhao, and K. B. Eisenthal, *Chem. Phys. Lett.* **191**, 327 (1992).
- ²⁴ Y. Dong, S. V. Pappu, and Z. Xu, *Anal. Chem.* **70**, 4730 (1998).
- ²⁵ C. D. Lorenz, P. S. Crozier, J. A. Anderson, and A. Travasset, *J. Phys. Chem. C* **112**, 10222 (2008).
- ²⁶ K. Leung, I. M. B. Nielsen, and L. J. Criscenti, *J. Am. Chem. Soc.* **131**, 18358 (2009).
- ²⁷ J. P. O'Reilly, C. P. Butts, I. A. I'Anso, and A. M. Shaw, *J. Am. Chem. Soc.* **127**, 1632 (2005).
- ²⁸ D. Desai, S. Karaman Didem, N. Prabhakar, S. Tadayon, A. Duchanoy, M. Toivola Diana, S. Rajput, T. Näreoja, and M. Rosenholm Jessica, *Open Mater.Sci.* **1**, 16 (2014).
- ²⁹ S. J. Manzano, D. Singappuli-Arachchige, B. L. Parikh, and I. I. Slowing, *Chem. Eng. J.* **340**, 73 (2018).
- ³⁰ Y.-C. Chen, A. Ostafin, and H. Mizukami, *Nanotechnol.* **21**, 215503 (2010).
- ³¹ G. G. Suchkova, and L. I. Maklakov, *Vib. Spectroscop.* **51**, 333 (2009).
- ³² J. Trébosc, J. W. Wiench, S. Huh, V. S. Y. Lin, and M. Pruski, *J. Am. Chem. Soc.* **127**, 3057 (2005).
- ³³ M. M. Kohonen, M. E. Karaman, and R. M. Pashley, *Langmuir* **16**, 5749 (2000).
- ³⁴ X.-D. Xiao, V. Vogel, and Y. R. Shen, *Chem. Phys. Lett.* **163**, 555 (1989).
- ³⁵ T. Sen, and M. Barisik, *Sci. Rep.* **9**, 137 (2019).
- ³⁶ T. Sen, and M. Barisik, *Phys. Chem. Chem. Phys.* **20**, 16719 (2018).

- ³⁷ C. De Stefano, O. Giuffrè, and S. Sammartano, *J. Chem. Eng. Data* **50**, 1917 (2005).
- ³⁸ S. Valetti, A. Feiler, and M. Trulsson, *Langmuir* **33**, 7343 (2017).
- ³⁹ E. Anderson, and T. H. Fife, *J. Am. Chem. Soc.* **95**, 6437 (1973).